Original scientific paper
https://doi.org/10.33180/InfMIDEM2024.305

Informacije MIDEM
Journal of Microelectronics,
Electronic Components and Materials
Vol. 54, No. 3(2024), 215 – 223

Preparation of Dielectric Layers for Applications in Digital Microfluidic Thermal Switches

Blaž Velkavrh[1,2,3,], Urban Tomc[2], Matej Šadl[1], Victor Regis[1,3], Maja Koblar[1], Bianka Colarič[2], Andrej Kitanovski[2] and Hana Uršič[1,3,*]*

[1]Jožef Stefan Institute, Electronic Ceramics Department, Ljubljana, Slovenia
[2]University of Ljubljana, Faculty of Mechanical Engineering, Ljubljana, Slovenia
[3]Jožef Stefan International Postgraduate School, Ljubljana, Slovenia

Abstract: In this work, we prepared dielectric layers of three different dielectric materials – Al_2O_3, polyimide and epoxy-based photopolymer SU-8 and investigated their properties. Aerosol deposition method was used to prepare Al_2O_3 and polyimide layers, while spin-coating method was used for SU-8 layers. Microstructural analysis revealed dense layers with no anomalies. Temperature- and frequency-independent dielectric permittivity ε' was observed for Al_2O_3 and SU-8 layers, while there was slight downside trend with increasing temperature for polyimide layers. According to Young-Lippmann equation of electrowetting on dielectric (EWOD) effect, Al_2O_3 is considered to be the best due to highest ε' (~11) among all three materials, since it requires the lowest voltage to achieve certain droplet contact angle with EWOD.

Keywords: dielectric layers, aerosol deposition method, spin-coating method, microfluidics, thermal switch

Priprava dielektričnih plasti za uporabo v digitalnih mikrofluidnih toplotnih stikalih

Izvleček: V tem raziskavi smo pripravili dielektrične plasti iz treh dielektričnih materialov – Al_2O_3, poliimid in fotopolimer na osnovi epoksida SU-8 ter raziskali njihove lastnosti. Za pripravo Al_2O_3 in poliimidnih plasti je bila uporabljena metoda nanašanja v aerosolu, za plasti SU-8 pa metoda nanašanja z vrtenjem. Mikrostrukturna analiza je pokazala goste plasti. Pri plasteh Al_2O_3 in SU-8 smo opazili temperaturno in frekvenčno neodvisno dielektričnost ε', medtem ko je pri poliimidnih plasteh viden rahlo padajoč trend z naraščajočo temperaturo. V skladu z Young-Lippmannovo enačbo učinka elektro-omočenja na dielektriku (EWOD) je Al_2O_3 zaradi najvišjega ε' (~11) smatran za najbolj ustrezen material za uporabo v EWOD, saj zahteva najnižjo napetost za doseganje določenega kontaktnega kota kapljice z EWOD.

Ključne besede: Dielektrične plasti, metoda nanašanja v aerosolu, metoda nanašanja z vrtenjem, mikrofluidika, toplotno stikalo

** Corresponding Author's e-mail: blaz.velkavrh@ijs.si, hana.ursic@ijs.si*

1 Introduction

The manufacture of electronic, optical, and mechanical devices is experiencing a continuous trend of miniaturization, making devices small and compact, as well as increasing their power density and efficiency. One of the main techniques for manufacturing miniaturized electronic devices in large volumes is multilayer technology, where layered structures are deposited on a substrate/board. These structures are prepared with additive processes and can consist of several conductive, semiconductive, or insulating dielectric layers with a typical thickness above 1 μm. The layers can be manufactured with different methods, for example powder-based technologies like screen-printing [1–3] and aerosol deposition (AD) [4–6], or solution-based like spin-coating method [7–9].

How to cite:
B. Velkavrh et al., "Preparation of Dielectric Layers for Applications in Digital Microfluidic Thermal Switches", Inf. Midem-J. Microelectron. Electron. Compon. Mater., Vol. 54, No. 3(2024), pp. 215–223

Advances in miniaturization have opened new problems of thermal management in small devices. With high power densities of compact devices, conventional heat sinks in combination with fans, heat pipes, or water cooling are insufficient to dissipate large amounts of heat to the ambient on a small scale. Potential solutions to improve thermal management on a smaller scale include thermal control devices, one of which is a digital microfluidic thermal switch based on electrowetting on dielectric (EWOD) effect [10–12]. Such a thermal switch requires a multilayer structure, consisting of a dielectric layer sandwiched between two electrode layers. The fabrication process of the dielectric layer has strong implications on its dielectric and thermal properties, which are a crucial factor in the performance of the thermal switch based on EWOD effect.

In this work, we investigated three different dielectric materials for EWOD applications. These three materials are alumina (Al_2O_3), polyimide, and epoxy-based photopolymer. Al_2O_3 was chosen due to its high electrical insulation, chemical inertness, and good mechanical properties [13–16]. On the other hand, dielectric polymers are low-cost materials with high electrical insulation [17]. The dielectrics were prepared in layer forms using AD (Al_2O_3 and polyimide) or spin-coating method (epoxy-based photopolymer) and their impacts on the voltage-dependent droplet contact angle were estimated by theoretical calculations.

2 Materials and methods

For preparation of dielectric layers, three different precursors were used, namely Al_2O_3 powder (A 16 SG, Almatis, Germany), polyimide powder (P84 NT, Evonik, Germany) and epoxy-based photopolymer SU-8 (GM1070, Gersteltec, Switzerland). Al_2O_3 and polyimide layers were prepared with the AD method, while epoxy-based photopolymer SU-8 layers were prepared with the spin-coating method. For preparation of polyimide and epoxy-based photopolymer SU-8 layers, both precursors were used as received, while Al_2O_3 powder needed a pre-treatment to achieve a high deposition rate and homogeneous microstructure without large pores as reported in [14, 18].

Raw Al_2O_3 powder was first thermally pre-treated in a chamber furnace (Custom-made, Terna, Slovenia) at 1150 °C for 1 h with 5 K min^{-1} heating and cooling rates, as suggested in [6, 14]. After thermal treatment, the powder was milled to obtain an appropriate particle size for AD, which is reported to be between 0.2 µm and 2 µm for the ceramic powders [4]. In our case, the d_{50} of the Al_2O_3 powder was 0.6 µm, as shown in Supplementary material: Figure S1. The milling was performed in a planetary mill (PM400, Retsch, Germany) at 200 min^{-1} for 4 h, using yttria-stabilized zirconia milling balls with isopropanol as a liquid medium.

For the preparation of dielectric layers, different substrates were chosen to optimize the deposition rate. Commercially available stainless-steel substrates (SS; no. 304, American Iron and Steel Institute) with a polished surface (A480: no. 8, American Society for Testing and Materials) were used for the ceramic Al_2O_3 dielectric layers, as it had previously been shown that a high deposition rate of the ceramic powder can be achieved on these substrates [19, 20]. For polyimide and epoxy-based photopolymer SU-8 layers, glass was used as a substrate. Cr/Au bottom electrodes with a thickness of ~100 nm were sputtered on the glass substrates by a magneton sputtering (Cinquepascal SRL, Italy).

The AD equipment was provided by Invertech, Germany. The process parameters during the AD for both Al_2O_3 and polyimide powders are gathered in Table 1.

For the spin-coating process, a spin-coater (WS-650MZ-23NPPB, Laurell, USA) was used to prepare epoxy-based photopolymer SU-8 layers. For better adhesion of epoxy-based photopolymer SU-8 on a gold-sputtered glass substrate, an adhesion promoter Omni-Coat (G112850, Kayaku Advanced Materials, USA) was used. During the preparation process, samples were thermally treated with an electric heater (C-MAG HS 7, IKA, Germany), according to instructions in the technical datasheet of epoxy-based photopolymer SU-8 [21]. The deposition was performed once without any repetition. The whole process is schematically presented in Figure 1.

Table 1: Aerosol deposition process parameters.

Process parameters	Value
Pressure in aerosol chamber [mbar]	<10
Nozzle slit size [mm^2]	(0.5 × 10)
Carrier gas	N_2
Gas flow rate [L min^{-1}]	2 – 4
Nozzle-substrate distance [mm]	5
Sweep speed [mm s^{-1}]	10

The thickness and root-mean-square roughness (R_q) of the prepared layers were evaluated from line profiles, measured with a contact profilometer (DektakXT, Bruker, USA). Thickness was determined from the step height of the layer, while R_q was evaluated with filtering the total profile using Gaussian regression with a cut-off 0.08 mm.

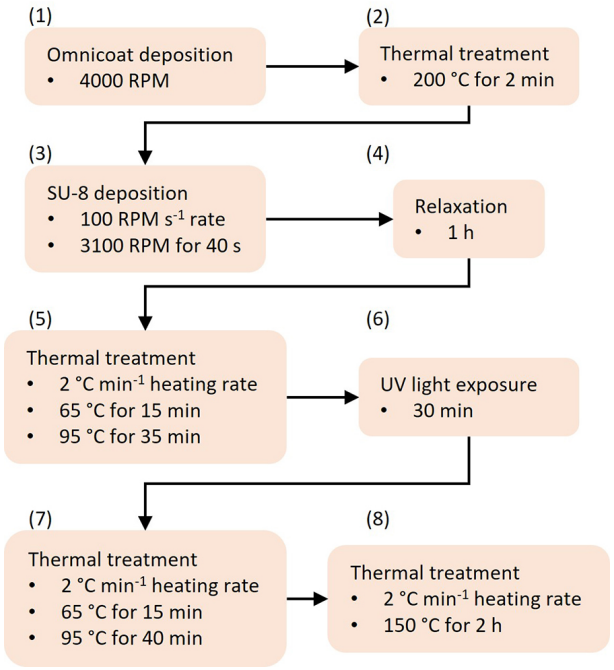

Figure 1: Schematic presentation of epoxy-based photopolymer SU-8 preparation process (after [21, 22]).

The topography images of the prepared dielectric layers were determined with the atomic force microscopes (AFM; Jupiter XR and MFP 3D, Asylum Research AFM, Oxford Instruments, USA). Images were scanned in AC air topography mode using tetrahedral platinum-coated silicon tips (OMCL-AC240TM-R3, Olympus, Japan). Prepared sample surfaces and their polished cross-sections were further investigated with scanning electron microscope (SEM; Verios G4 HP, Thermo Fisher Scientific, USA). To analyse the layers in cross-section, the samples were prepared by cutting, mounting in epoxy resin (EpoFixKit, Struers, Denmark), grinding, and fine polishing using a colloidal SiO_2 suspension (OP-S, Struers, Denmark).

For dielectric measurements, Au electrodes with a 0.5 mm diameter were sputtered on the top surface of prepared dielectric layers by a magneton sputtering (Cinquepascal SRL, Italy). The temperature-dependent dielectric permittivity ε' and dielectric losses tan(δ) were measured with Aixacct TF Analyzer 2000 (Aixacct Systems GMbH, Germany) and a HP 4284 A Precision LCR impedance meter (Hewlett-Packard, USA), using AC amplitude of 1 V at different frequencies during cooling in the temperature range from 100 °C to -30 °C. Theoretical voltage-dependent contact angles for a water droplet were calculated with a Young-Lippmann equation [11].

3 Results

Dielectric layers were prepared from ceramic Al_2O_3, polyimide and epoxy-based photopolymer SU-8. The microstructural and electrical properties are shown first. Later, to determine the influence of the dielectric layers on EWOD effect, the voltage-dependent contact angles for a water droplet were calculated.

3.1 Al_2O_3 layers prepared by the aerosol deposition method

Figure 2a shows a photograph of an Al_2O_3 layer on a stainless-steel substrate. AFM height and tapping amplitude images and SEM images in Figure 2b–2e revealed a layer surface with the root-mean-square roughness $R_q \approx 40$ nm. The concave depressions commonly found in aerosol-deposited layers can be found in the AFM height image (Figure 2b). These surface characteristics are formed by collision of powder particles with the surface layer during the AD process, as discussed previously in [23]. SEM layer-surface images (Figure 2d and 2e) revealed small powder particles with a size in the range of nanometres as part of the Al_2O_3 layer surface. A comparison of the particle size of the Al_2O_3 powder before AD (Supplementary material: Figure S1) with the particles in the layers indicates that Al_2O_3 particles break during the AD process, as previously discussed in [6]. The cross-section SEM image in Figure 2f revealed a dense 4 µm-thick Al_2O_3 layer on a stainless-steel substrate. No large defects or pores are observed, similar to Al_2O_3 layers, previously prepared by the same procedure and deposited on gadolinium substrates, as reported in [6]. Temperature-dependent ε' measurements are shown in Figure 3. The ε' remains constant at ~11, independent of both temperature and frequency. The tan(δ) slightly increases with increasing temperature but remains below 0.02 over the entire measurement range.

3.2 Polyimide layers prepared by the aerosol deposition method

Figure 4a shows a photograph of polyimide layer on a gold-sputtered glass substrate. AFM height and tapping amplitude images and SEM images in Figure 4b–4e revealed a rough layer surface with $R_q \approx 1.4$ µm. The concave depressions commonly found in AD layers are also visible in this case (Figure 4b), but they are deeper than in Al_2O_3, resulting in a higher surface roughness. In SEM images of the polyimide layer surface (Figure 4d and 4e), particles with a size of several tens to hundreds of nanometres can be seen. In the SEM images of the polyimide powder before AD (Supplementary material: Figure S2), a similar particle size was observed,

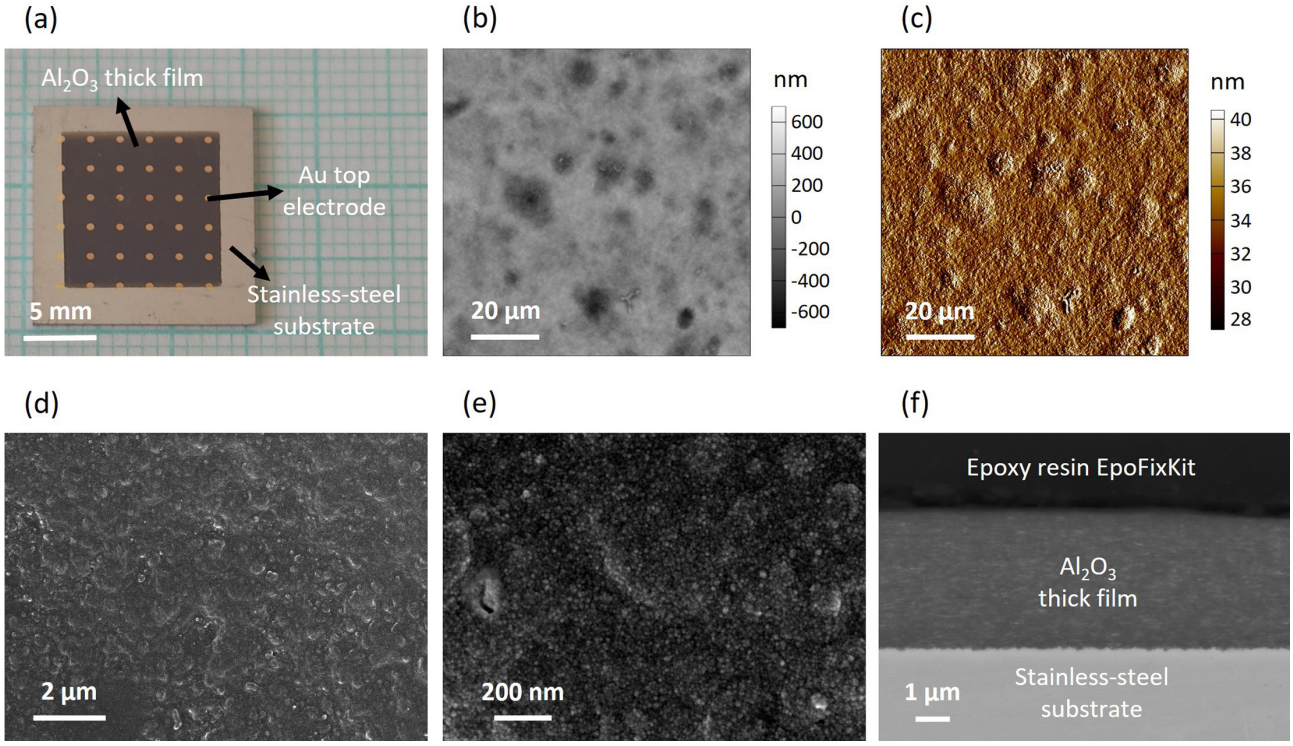

Figure 2: (a) Photograph of aerosol-deposited Al_2O_3 layer on stainless-steel substrate. AFM (b) height and (c) tapping mode amplitude images. SEM (d, e) surface and (f) cross-section images of the Al_2O_3 layer.

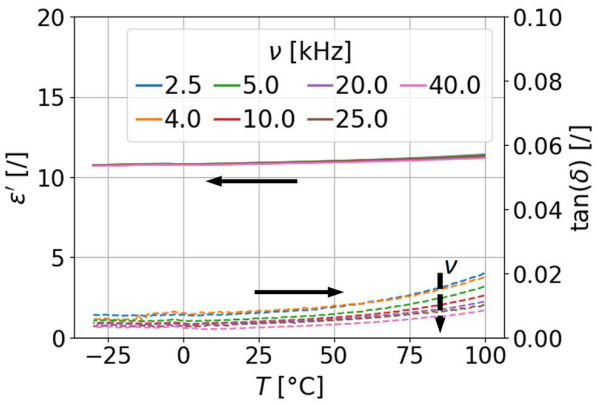

Figure 3: Temperature-dependent ε' and tan(δ) of Al_2O_3 layer at different frequencies. The vertical black dashed arrow indicates increase in frequency.

but these particles were mainly agglomerated. Similar particle size before and after AD indicates that particles were not heavily fractured during the AD process, in contrast to ceramic Al_2O_3 particles. During AD, the agglomerates of polyimide particles break apart, while polyimide particles deform and stick together, resulting in the formation of dense polyimide layers. The cross-section SEM image of such a dense polyimide layer with a thickness d ≈ 19 µm is shown in Figure 4f. No large anomalies or pores are visible through the layer thickness. We can observe slight delamination of the bottom electrode from the glass substrate, which is caused by mechanical forces arising from the curing process of the polymer epoxy-resin EpoFixKit during the cross-section sample preparation. Temperature-dependent ε' measurements are shown in Figure 5. The graph shows a slight downward trend of ε' with increasing temperature. No large frequency dependence is observed. On average, ε' remains at ~5.5. The tan(δ) slightly decreases with the increasing temperature but remains below 0.03 over the entire measurement range.

3.3 Epoxy-based photopolymer SU-8 layers prepared by spin-coating method

Figure 6a shows a photograph of epoxy-based photopolymer SU-8 layer on a gold-sputtered glass substrate. AFM height and tapping amplitude images as well as SEM surface images in Figure 6b–6e revealed a smooth layer surface with R_q ≈ 4 nm. While the SEM layer surface image at lower magnification (Figure 6d) does not reveal any details, SEM image at higher magnification (Figure 6e) shows small particles of epoxy-based photopolymer SU-8 with a size in nanometre range. The SEM cross-section image in Figure 6f revealed a dense layer with a thickness d ≈ 30 µm with no large anomalies or bubbles. Temperature-dependent ε' measurements are shown in Figure 7. The ε' remains constant at ~6.5, independent of both temperature and frequency. The tan(δ) slightly decreases

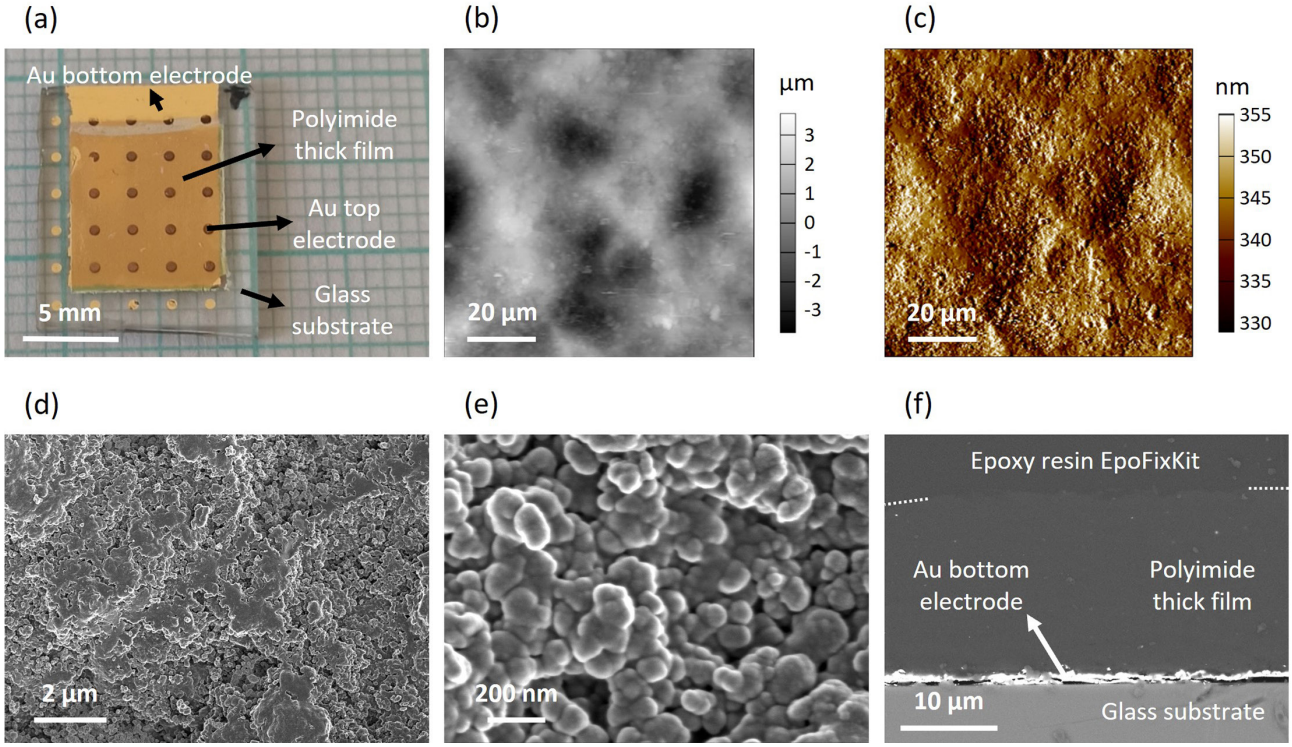

Figure 4: (a) Photograph of aerosol-deposited polyimide layer on gold-sputtered glass substrate. AFM (b) height and (c) tapping mode amplitude images. SEM (d, e) surface and (f) cross-section images of the polyimide layer. Please note that on panel (f), two white doted lines in the corners of the image between the polyimide layer and the epoxy resin EpoFixKit are only the guide for the eye.

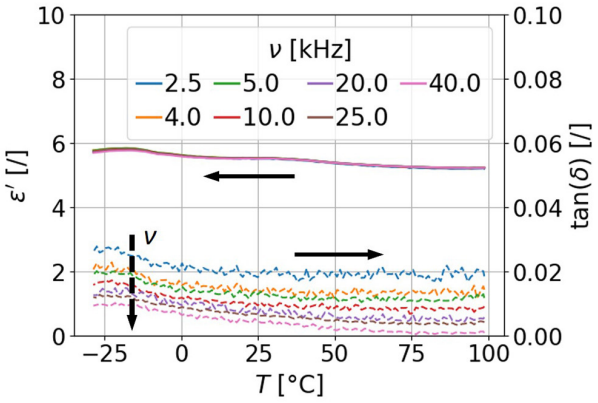

Figure 5: Temperature-dependent ε' and tan(δ) of polyimide layer at different frequencies. The vertical black dashed arrow indicates increase in frequency.

with increasing temperature, similar as in the case of polyimide layers (Figure 5). However, it remains below 0.05 over the entire measurement range.

3.4 Water droplet contact angles on dielectric layers

The roughness R_q and dielectric permittivity ε' of prepared layers are collected in Table 2. Polyimide layers prepared with AD method have the highest R_q, while epoxy-based photopolymer SU-8 layers, prepared with spin-coating method have the lowest R_q between all three different types of layers. In AD, powder particles collide with layer surface and form rougher surface in comparison to spin-coating method. When comparing Al_2O_3 and polyimide layers, both prepared with AD method, huge difference in roughness can be observed. While ceramic Al_2O_3 particles break during the AD process, forming the surface with lower roughness, polyimide particles deform and stick together, forming the surface with much higher roughness. The ceramic Al_2O_3 layers exhibited the highest dielectric permittivity ε' compared to both polyimide and epoxy-based photopolymer SU-8 layers.

Table 2: The root-mean-square surface roughness R_q and dielectric permittivity ε' of prepared dielectric layers.

	Aerosol deposition		Spin-coating
Material	Al_2O_3	Polyimide	SU-8
R_q [nm]	40	1400	4
ε' [/] @ 10 kHz	11	5.5	6.5

Figure 8 shows theoretical voltage-dependent water droplet contact angles on Al_2O_3, polyimide and epoxy-based photopolymer SU-8 layers. The voltage-dependent droplet contact angles of the water droplet were

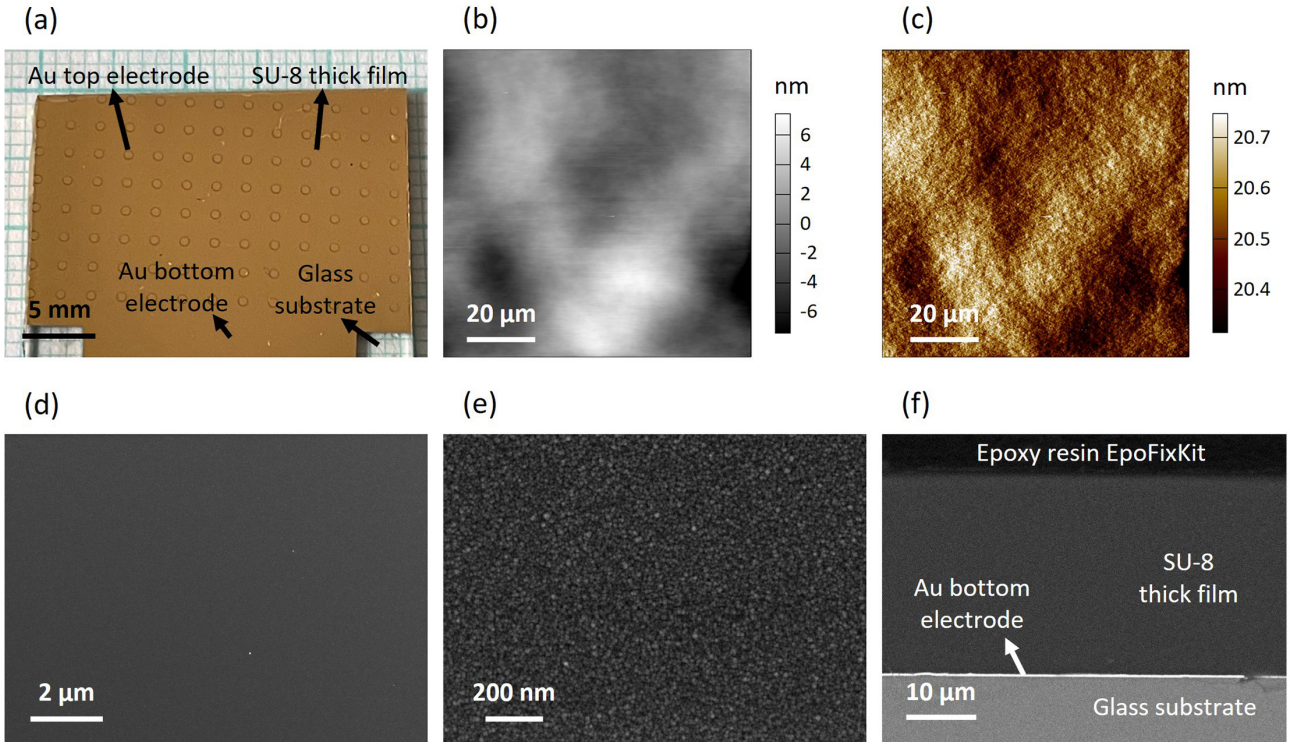

Figure 6: (a) Photograph of spin-coated epoxy-based photopolymer SU-8 layer on gold-sputtered glass substrate. AFM (b) height and (c) tapping mode amplitude images. SEM (d, e) surface and (f) cross-section images of the epoxy-based photopolymer SU-8 layer.

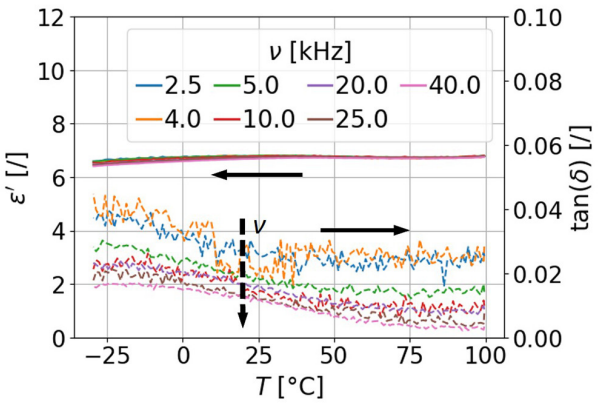

Figure 7: Temperature-dependent ε' and tan(δ) of epoxy-based photopolymer SU-8 layer at different frequencies. The vertical black dashed arrow indicates increase in frequency.

calculated according to Young-Lippmann equation [11]:

$$\cos\theta_{ew}(U) = \cos\theta_{eq} + \frac{\varepsilon_0 \cdot \varepsilon'}{2 \cdot d \cdot \gamma_{lv}} \cdot U^2 , \quad (1)$$

where ε' was taken from Table 2. The θ_{eq} is the initial droplet contact angle, θ_{ew} a contact angle when electric field is applied, ε_0 dielectric permittivity of a vacuum, U voltage, d thickness of the dielectric layer and γ_{lv} surface tension of a liquid droplet. For a water droplet in air atmosphere at room temperature, γ_{lv} = 0.072 N m^{-1} was used [24]. An additional hydrophobic layer can be applied on the top of the dielectric layer to achieve high θ_{eq}. Therefore, θ_{eq} = 120° was used according to technical datasheet of fluoropolymer FluoroPel 1601V (Cytonix, USA), commonly used for EWOD applications [25]. Graphs in Figure 8 indicate Al_2O_3 to be the best choice between all three materials for EWOD applications, since it has the highest ε', resulting in lower voltage required to obtain certain contact angle at chosen layer thickness d. However, Young-Lippmann equation assumes smooth and ideally flat surfaces, but the roughness of the dielectric layers also needs to be considered, since it influences the surface wettability – droplet contact angle [26]. In addition, the roughness also has the influence on the interface thermal resistances in the multilayer structure, which effects the heat transfer capabilities of digital microfluidic thermal switch based on EWOD effect. Therefore, SU-8 might also be appropriate due to lowest roughness, which would positively effect heat transfer capabilities of multilayer structure.

4 Conclusions

The microstructural and electrical properties of different dielectric layers were investigated and their influence on

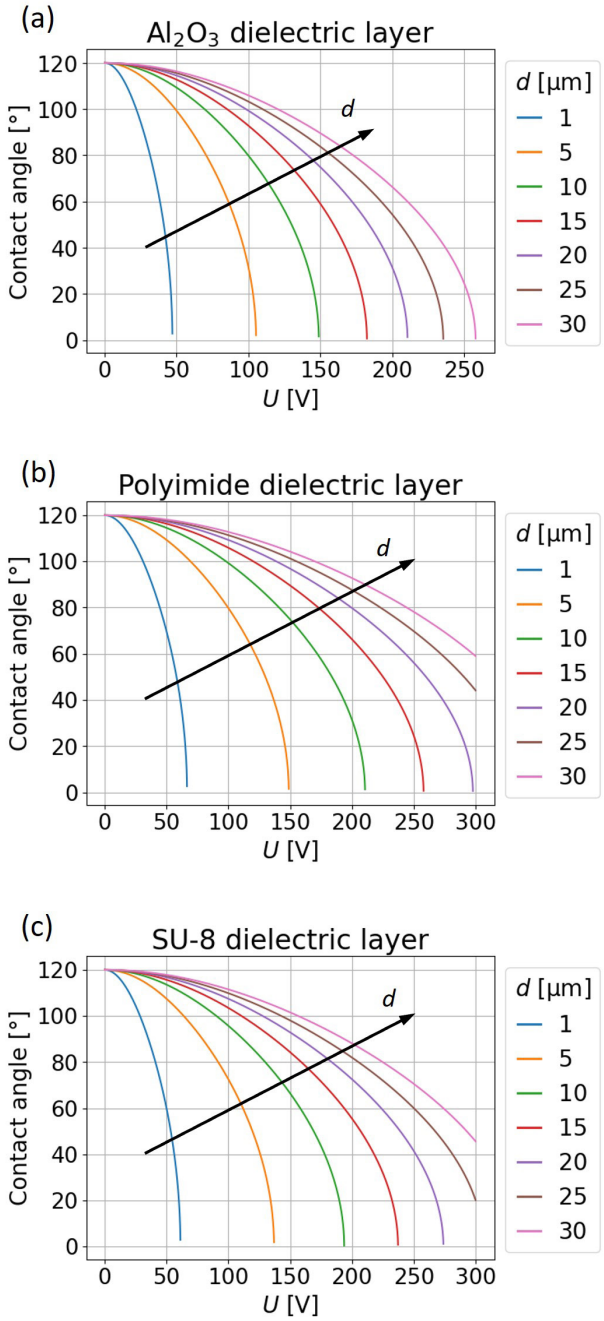

Figure 8: Theoretically calculated voltage-dependent contact angles for water droplets on (a) Al_2O_3, (b) polyimide and (c) epoxy-based photopolymer SU-8 layers at different dielectric layer thicknesses.

the EWOD effect was determined. Al_2O_3 and polyimide layers were prepared with AD method, while epoxy-based photopolymer SU-8 was prepared with spin-coating method. Microstructural analysis revealed dense layers without any anomalies. Particle analysis indicates breaking of ceramic Al_2O_3 particles during the AD process. In the case of polyimide, big agglomerates, observed in raw powder, break apart during the AD process, while smaller polyimide particles deform and stick together. Dielectric measurements revealed temperature- and frequency-independent dielectric permittivity ε' for Al_2O_3 and epoxy-based photopolymer SU-8, while slight temperature dependency of ε' can be observed in polyimide. Highest dielectric permittivity ε' between all three materials was measured in Al_2O_3 layers ($\varepsilon' \sim 11$), indicating Al_2O_3 as the optimal choice for EWOD application.

5 Supplementary material

Supplementary material available on the publisher's web page contains:

- S1: Particle size distribution and SEM analysis of Al_2O_3 powder
- S2: Particle size distribution and SEM analysis of polyimide powder

6 Acknowledgments

The authors acknowledge financial support from the transnational consortium M-ERA.NET for the project Cool BatMan: Battery Thermal Management System Based on High Power Density Digital Microfluidic Magnetocaloric Cooling (No. 9400, Slovenian part of the project is financed by Ministry of Higher Education, Science and Innovation). Authors also acknowledge the financial support of the Slovenian Research and Innovation Agency for the research core fundings (No. P2-0422, P2-0223, J2-1738-1 and P2-0105). The assistance of Jena Cilenšek, Val Fišinger, Brigita Kmet and Andreja Benčan is gratefully acknowledged.

7 Conflict of interest

The authors declare no conflict of interest. The founding sponsors had no role in the design of the study; in the collection, analyses, or interpretation of data; in the writing of the manuscript, and in the decision to publish the results.

8 References

1. R. Dorey, *Ceramic Thick Films for MEMS and Microdevices*. 2011. https://doi.org/10.1016/C2009-0-20338-2.
2. M. Kosec, D. Kuscer, and J. Holc, "Processing of ferroelectric ceramic thick films," *Springer Series in Materials Science*, vol. 140, no. 1, 2011, https://doi.org/10.1007/978-90-481-2875-4_2.

3. B. Malič, D. Kuščer, M. Vrabelj, and J. Koruza, "Review of methods for powder-based processing," in *Magnetic, Ferroelectric, and Multiferroic Metal Oxides*, 2018. https://doi.org/10.1016/B978-0-12-811180-2.00005-0.
4. D. Hanft, J. Exner, M. Schubert, T. Stöcker, P. Fuierer, and R. Moos, "An overview of the Aerosol Deposition method: Process fundamentals and new trends in materials applications," *Journal of Ceramic Science and Technology*, vol. 6, no. 3. 2015. https://doi.org/10.4416/JCST2015-00018.
5. J. Akedo, "Room temperature impact consolidation (RTIC) of fine ceramic powder by aerosol deposition method and applications to microdevices," *Journal of Thermal Spray Technology*, vol. 17, no. 2. 2008. https://doi.org/10.1007/s11666-008-9163-7.
6. M. Sadl, U. Tomc, and H. Ursic, "Investigating the feasibility of preparing metal–ceramic multi-layered composites using only the aerosol-deposition technique," *Materials*, vol. 14, no. 16, 2021, https://doi.org/10.3390/ma14164548.
7. T. Schneller, R. Waser, M. Kosec, and D. Payne, *Chemical solution deposition of functional oxide thin films*. 2013. https://doi.org/10.1007/978-3-211-99311-8.
8. K. Norrman, A. Ghanbari-Siahkali, and N. B. Larsen, "Studies of spin-coated polymer films," *Annual Reports on the Progress of Chemistry - Section C*, vol. 101. 2005. https://doi.org/10.1039/b408857n.
9. T. Pečnik, S. Glinšek, B. Kmet, and B. Malič, "Combined effects of thickness, grain size and residual stress on the dielectric properties of $Ba_{0.5}Sr_{0.5}TiO_3$ thin films," *J Alloys Compd*, vol. 646, 2015, https://doi.org/10.1016/j.jallcom.2015.06.192.
10. K. Klinar, T. Swoboda, M. Muñoz Rojo, and A. Kitanovski, "Fluidic and Mechanical Thermal Control Devices," *Advanced Electronic Materials*, vol. 7, no. 3. 2021. https://doi.org/10.1002/aelm.202000623.
11. F. Mugele and J. Heikenfeld, *Electrowetting: Fundamental Principles and Practical Applications*. Wiley-VCH, 2018. https://doi.org/10.1002/9783527412396.
12. S. K. Cho, H. Moon, and C. J. Kim, "Creating, transporting, cutting, and merging liquid droplets by electrowetting-based actuation for digital microfluidic circuits," *Journal of Microelectromechanical Systems*, vol. 12, no. 1, 2003, https://doi.org/10.1109/JMEMS.2002.807467.
13. T. Lampke *et al.*, "Corrosion and wear behavior of alumina coatings obtained by various methods," *Materials Science*, vol. 46, no. 5, 2011, https://doi.org/10.1007/s11003-011-9328-2.
14. M. Sadl, U. Tomc, U. Prah, and H. Ursic, "Protective alumina coatings prepared by aerosol deposition on magnetocaloric gadolinium elements," *Informacije MIDEM*, vol. 49, no. 3, 2019, https://doi.org/10.33180/infmidem2019.306.
15. M. Linz, J. Exner, T. Nazarenus, J. Kita, and R. Moos, "Mobile sealing and repairing of damaged ceramic coatings by powder aerosol deposition at room temperature," *Open Ceramics*, vol. 10, 2022, https://doi.org/10.1016/j.oceram.2022.100253.
16. B. Xie, Y. Li, J. Pan, and D. A. Hall, "Process optimisation of alumina coatings by modification of powder characteristics in the aerosol deposition method," *J Eur Ceram Soc*, vol. 44, no. 5, pp. 3147–3157, 2024, https://doi.org/10.1016/j.jeurceramsoc.2023.12.085.
17. H. P. Palani Velayuda Shanmugasundram, E. Jayamani, and K. H. Soon, "A comprehensive review on dielectric composites: Classification of dielectric composites," *Renewable and Sustainable Energy Reviews*, vol. 157. 2022. https://doi.org/10.1016/j.rser.2022.112075.
18. V. Regis, M. Šadl, G. Brennecka, A. Bradeško, U. Tomc, and H. Uršič, "Investigation of Structural and Electrical Properties of Al2O3/Al Composites Prepared by Aerosol Co-Deposition," *Crystals (Basel)*, vol. 13, no. 5, 2023, https://doi.org/10.3390/cryst13050850.
19. M. Sadl *et al.*, "Energy-storage-efficient $0.9Pb(Mg_{1/3}Nb_{2/3})O_3$–$0.1PbTiO_3$ thick films integrated directly onto stainless steel," *Acta Mater*, vol. 221, 2021, https://doi.org/10.1016/j.actamat.2021.117403.
20. N. H. Khansur, U. Eckstein, L. Benker, U. Deisinger, B. Merle, and K. G. Webber, "Room temperature deposition of functional ceramic layers on low-cost metal substrate," *Ceram Int*, vol. 44, no. 14, 2018, https://doi.org/10.1016/j.ceramint.2018.06.027.
21. Gersteltec Sàrl, "Technical Datasheet GM1070." Accessed: Feb. 01, 2024. [Online]. Available: https://www.gersteltec.ch/su8/
22. M. T. Hong *et al.*, "The Effect of Bake Temperature on SU-8 Gate Insulator of IGZO Thin Film Transistor," *Journal of the Korean Physical Society*, vol. 73, no. 3, 2018, https://doi.org/10.3938/jkps.73.297.
23. D. W. Lee, H. J. Kim, and S. M. Nam, "Effects of starting powder on the growth of Al_2O_3 films on Cu substrates using the aerosol deposition method," *Journal of the Korean Physical Society*, vol. 57, no. 41, 2010, https://doi.org/10.3938/jkps.57.1115.
24. The Engineering ToolBox, "Surface Tension - Water in contact with Air." Accessed: Feb. 04, 2024. [On-

line]. Available: https://www.engineeringtoolbox.com/water-surface-tension-d_597.html
25. Cytonix, "FluoroPel PFC1601V." Accessed: Mar. 05, 2024. [Online]. Available: https://cytonix.com/products/1601v
26. X. Wang and Q. Zhang, "Role of surface roughness in the wettability, surface energy and flotation kinetics of calcite," *Powder Technol*, vol. 371, 2020, https://doi.org/10.1016/j.powtec.2020.05.081.

Arrived: 13. 05. 2024
Accepted: 18. 07. 2024